Electric Power Systems Research 235 (2024) 110854

Contents lists available at ScienceDirect

Electric Power Systems Research

journal homepage: www.elsevier.com/locate/epsr

Adaptive parameter tuning strategy of VSG-based islanded microgrid under uncertainties

Himanshu Grover [a,*], Sumedha Sharma [b], Ashu Verma [c], M.J. Hossain [d], Innocent Kamwa [a]

[a] Department of Electrical and Computer Engineering, University Laval, Quebec, Canada
[b] Department of Electrical and Software Engineering, University of Calgary, Alberta, Canada
[c] Department of Energy Science and Engineering, Indian Institute of Technology Delhi, India
[d] School of Electrical and Data Engineering, University of Technology, Sydney, Australia

ARTICLE INFO

Keywords:
Virtual synchronous generator
Solar PV
Robust control
Stochastic optimization
Frequency regulation

ABSTRACT

This paper proposes adaptive parameter tuning strategy for a virtual-synchronous generator (VSG) during islanding conditions to improve frequency oscillations occurring due to uncertainties in load and solar photovoltaic (PV) output. Accordingly, an adaptive two-level optimization model has been developed for optimal tuning of VSG parameters. It provides dynamic virtual inertia value to VSG by maintaining rate-of-change-of-frequency (RoCoF) within prescribed limits under disturbance. The first level calculates the initial value of VSG parameters using robust control considering day-ahead operation schedules and uncertainty information. During intra-day operation stage on the following day, as soon as islanding is detected, the VSG is operated with robust values of the parameters computed day ahead at the first level. Furthermore, during islanded operation, second level utilizes initial values from first level and determines expectation values of short-leading-time predictions of PV output and load, and performs an adaptive stochastic optimization of VSG parameters in intervals of 5 min. Extensive simulations have been performed to evaluate the performance of proposed adaptive parameters tuning strategy on modified Cigre European LV network. Furthermore, effectiveness of proposed control approach has been validated on laboratory-scale hardware experimental setup under uncertain environments and cyber-attack. Results reveal improved performance of adaptive VSG in regulating network frequency in presence of system uncertainties.

1. Introduction

The concept of microgrids (MG) has become an emerging trend in modern electrical systems due to large-scale integration of renewable energy (RE) based distributed energy resources (DERs) along with smart control and communication infrastructure. Such microgrids have the capability to operate in grid-connected or islanded modes [1]. During grid-connected operation, the frequency and voltage of microgrids are regulated by the utility grid, whereas during islanded operation, grid-forming sources such as diesel generators, energy storage-based voltage source converters (VSC), etc. regulate the microgrid system frequency and voltage. However, such microgrids inevitably face frequency and voltage stability issues during islanded operation due to their low-inertia.

Reduction in system inertia leads to undesirable triggering of protection systems such as rate-of-change-of-frequency (RoCoF) relays and under/over frequency relays, due to real-time uncertainty in solar photovoltaic (PV) output and load variability [2,3]. Such unwanted activation of the protection system may result in system breakdowns and microgrid blackouts. In view of this, recent research works have investigated control strategies to counteract the stability concerns arising in high RES-penetrated electrical networks through fast control strategies for diesel generators [4], inertial support through battery energy storage systems (BESS) based VSC [5–7] and smart loads [8].

In this context, numerous studies have been carried out to rapidly mitigate the power mismatch and regulate the microgrid frequency through BESS-based VSG control. BESS-based grid-forming converters can be utilized to enhance system stability during transient conditions through virtual inertia support. Various control methods for incorporating virtual inertia in MGs, such as synchronous generator (SG) model-based, swing equation-based, frequency-power response-based, and droop-based approaches, have been proposed in [9–11]. However, the droop-based approach presented in [11], does not include the ability to provide inertia support for the microgrid during disturbances. The

* Corresponding author.
E-mail address: groverhimanshu.ee@gmail.com (H. Grover).

https://doi.org/10.1016/j.epsr.2024.110854
Received 21 February 2024; Received in revised form 7 June 2024; Accepted 26 June 2024
Available online 17 July 2024

work presented in [12] establishes that VSG control mimics the identical behaviour of SG and provides inertial support during any disturbance in the system. VSG-based VSC control reduces frequency deviation (f_{nadir}), improves RoCoF and provides faster frequency restoration during power disturbances.

A significant distinction between the SG and VSG-based VSC is that the VSG-based VSC is a power electronics device that offers flexible operation as its inertial response may be controlled by adjusting the control parameters. Accordingly, [13,14] depicts the effects of VSG parameters on its inertial response. It is observed that the higher values of inertia constant result in lower frequency deviations, and large oscillations with longer settling time. However, lower values of inertia constant would adversely affect system stability by increasing RoCoF and frequency deviation with fewer oscillations and faster settling time. Therefore, the VSG parameters must be selected carefully such that it results in lower frequency deviation and faster settling time thereby maintaining the RoCoF within prescribed limits. Furthermore, in general practice the VSG parameters are selected depending on the largest disturbance expected in the system. However, VSG parameters calculated based on the largest power disturbance may deteriorate system performance when faced with smaller disturbances. Moreover, it is noteworthy that the first frequency oscillation following a power disturbance is the most crucial in terms of maintaining system stability which is majorly dependent on VSG parameters. However, optimal selection of VSG parameters to address the power disturbance arising out of PV output and load uncertainty would require estimation of the expected power disturbance prior to its actual occurrence. Accordingly, it would be appropriate to precisely model system uncertainties expected during real-time operation to optimally select the VSG parameters.

Various configurations of VSG have been found in the literature [15–21]. In the present work, a cascade-type VSG configuration was chosen as given in [21]. Utilizing cascade-type VSGs offers a revolutionary method to improve grid stability and incorporate renewable energy sources. Cascade-type VSGs enhance the resilience of power systems against temporary disruptions by imitating the characteristics of conventional synchronous generators, resulting in greater inertia and frequency management. Their capacity to function as grid-forming entities allows for the smooth incorporation of renewable energy, hence addressing the difficulties related to intermittency and variability. In addition, cascade-type VSGs offer versatile functionality, quick response times, and the ability to be customized to suit various grid setups and operating needs. Cascade-type VSGs play a crucial role in improving the reliability, efficiency, and sustainability of modern power grids by enabling islanded operation and enhancing power quality.

Several recent research works have focused on adaptive VSG tuning and control [22–27]. The authors in [22], proposed an adaptive VSG control to optimize system inertia while considering storage and converter capacity into account. A small-signal modelling and parameter designing approach for VSG has been presented in [23]. An improved virtual inertia control approach was introduced in [24], to simultaneously achieve precise steady state active power regulation and improved dynamic response. The authors in [25], proposed a dual-adaptive virtual inertia control technique to achieve a balance between active power management and frequency regulation. Self-adaptive inertia and damping combination control method have been proposed in [26], for enhancing frequency stability using an interleaving control mechanism. The authors in [27], proposed an adaptive virtual inertia control that improves the dynamic performance of the system by providing large inertia when system frequency crosses a normal threshold value. It is observed that while most of the above-mentioned papers highlight the need and develop techniques for adaptive VSG control and parameter tuning, the parameters thus obtained might not be optimized for practical operating conditions. Moreover, since RoCoF and inertia constant are inversely related, it is desirable to obtain an optimal trade-off between the two values for seamless VSG operation, thereby highlighting the need to develop optimization strategies for adaptive parameters tuning of VSG-based VSC.

In this context, some recent papers have focused on optimization for evaluation of VSG parameters [1,13,28,29]. It is observed that the works in [1,28], utilize particle swarm optimization for computing VSG parameters. However, metaheuristic algorithms often suffer from inconsistent solutions, higher computational times, and difficulty in rigorously converging. Thus, these solution algorithms often appear unfit for short-timescale operational problems such as determining VSG parameters under real-time uncertainties. Further, a self-tuning virtual synchronous machine for optimization of the VSG parameters through direct-search method has been proposed in [13]. The proposed control optimizes the VSG parameters when needed to reduce settling time and power flow from BESS. Another work presented in [29], proposes a multi-objective optimization for tuning of VSG parameters with high RES penetration. However, most of the existing works do not consider the effect of RES and load uncertainties occurring during actual system operation. It must be noted that since the system inertia in RES-penetrated networks is reduced, they become more susceptible to instability due to power fluctuations. To the best of the authors' knowledge, existing works do not incorporate uncertainty modelling and pre-disturbance estimation for adaptive tuning of VSG parameters during the islanding mode of microgrid.

In view of the aforementioned discussion, this paper develops an adaptive optimization approach for tuning of VSG parameters for frequency regulation in islanded microgrids, considering uncertainty in loads and RES output. Major contributions are summarized as follows.

(1) Development of adaptive parameters tuning strategy using two-level optimization for optimal tuning of VSG in islanding operation to avoid undesirable triggering of the protection system for low-inertia microgrids.

(2) The developed two-level adaptive optimization framework evaluates robust VSG parameters day-ahead, followed by a stochastic programming model for adaptive multi-objective optimization of VSG parameters to counteract the effects of system uncertainties in shorter timescales upon islanding.

(3) The performance of the proposed adaptive parameters tuning strategy has been evaluated through extensive simulations on a modified cigre European LV network.

(4) Effectiveness of the proposed adaptive parameters tuning strategy has been validated in a laboratory-scale experimental setup under an uncertain environment and cyber-attack.

The remainder of this paper is organized as follows. The system description is provided in Section 2. Section 3 describes the adaptive parameters tuning strategy. Section 4 illustrates mathematical modelling. Simulation results are depicted in Section 5 and experimental results are depicted in Section 6. Finally, the conclusion of the research work is drawn in Section 7.

2. System description

An overview of the proposed smart microgrid system is shown in Fig. 1. The microgrid system consists of three-phase low-voltage distribution network with different types of buildings such as commercial, residential etc. The buildings include smart metering infrastructure which measures the electrical parameters of each building and transmits the data to the cloud database using Internet-of-Things (IoT) communication infrastructure. The data stored in cloud database is monitored by central controller of microgrid control centre (MGCC) through energy internet paradigm. The buildings are also equipped with different types of loads and roof-top solar PV generators. Primarily the microgrid is powered by the grid through substation, and solar PV generator operates in grid following mode. However, during islanded mode of operation, the microgrid isolates from the grid network, and VSG-based VSC acts as the master source for the microgrid. The VSG-based VSC consists of BESS connected to the DC bus of VSC through

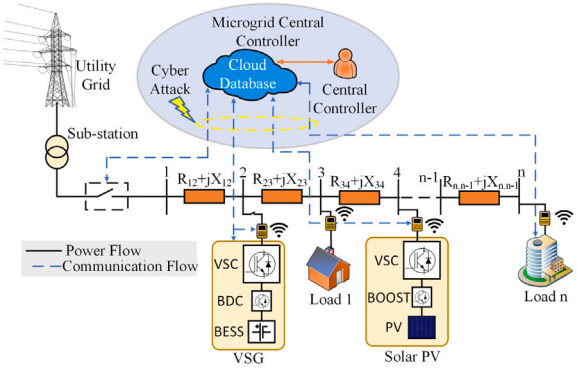

Fig. 1. Overview of the proposed smart microgrid system.

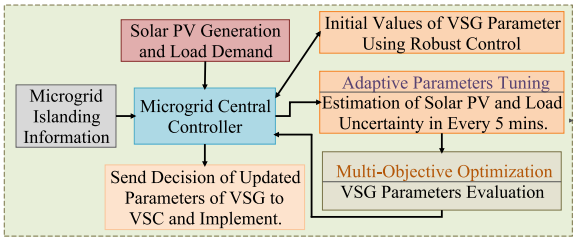

Fig. 2. Proposed adaptive parameters tuning strategy.

bi-directional DC–DC converter, and regulates microgrid system frequency and voltage by supplying power to the loads. The VSCs of solar PV generators operate as slaves and follow the frequency and voltage generated by the VSG-based VSC.

3. Adaptive parameters tuning strategy

An adaptive parameter tuning strategy for VSG has been proposed to regulate the frequency and voltage of RES-integrated microgrid systems. Owing to the occurrence of uncertainties and multiple modes of microgrid operation, the proposed control has been proposed for an islanded mode of operation. The framework of the proposed adaptive parameter tuning strategy is shown in Fig. 2. During islanded mode, VSG converter provides virtual inertia to the system by mimicking the dynamic characteristics of synchronous generator. The microgrid islanding information along with solar PV generation and load demand is sent to the MGCC. The MGCC evaluates robust values of VSG parameters by considering day-ahead operation schedules and uncertainty information. In real-time during islanded operation, an optimization scheme has been developed to evaluate optimal values of VSG parameters every 5-minute intervals, based on the expectation of solar PV and load uncertainties through the stochastic programming approach. The decision of VSG parameters is communicated to VSG-based VSC for seamless operation during islanded microgrid. The detailed explanation of the above control is explained in successive sections.

4. Mathematical modelling

4.1. Virtual synchronous generator (VSG)

The proposed two-stage VSG control based VSC is shown in Fig. 3. It consists of BESS, DC–DC Bi-directional converter (BDC) and a VSC. The VSC is interlinked to point-of-common (PCC) coupling through step-up transformer and line impedance. The BESS regulates the DC bus voltage through BDC using voltage-current control loops. The control signals (S_7&S_8) of BDC for DC bus voltage control are calculated using the following equations [30].

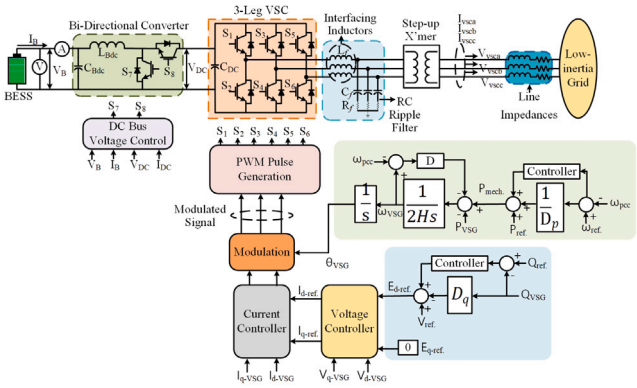

Fig. 3. Microgrid configuration of BESS based VSG.

$$\Delta V_{DC} = V_{DCref} - V_{DC}\left(\frac{2\pi f_{cf}}{s+2\pi f_{cf}}\right) \tag{1}$$

$$I_{Bref}(t) = k_{pdc}\Delta V_{DC} + k_{idc}\int \Delta V_{DC}.dt \tag{2}$$

$$\Delta I_B = I_{Bref} - I_B\left(\frac{2\pi f_{cf}}{s+2\pi f_{cf}}\right) \tag{3}$$

$$D_B = k_{pb}\Delta I_B + k_{ib}\int \Delta I_B.dt \tag{4}$$

where V_{DC} is the actual DC bus voltage which is passed through low-pass filter (LPF), whose cut-off frequency (f_{cf}) is chosen as 5 Hz. V_{DCref} is the reference DC bus voltage, ΔV_{DC} is the change in DC bus voltage. k_{pdc} and k_{idc} are the proportional and integral gain constant of outer voltage control loop respectively. I_{Bref} is the reference battery current calculated from outer voltage control loop and I_B is the actual battery current. ΔI_B is the difference in reference and actual battery current. k_{pb} and k_{ib} are the proportional and integral gain constant of inner current control loop respectively. D_B is the duty cycle for bi-directional DC–DC converter which is converted to pulse width modulating (PWM) signals (S_7&S_8) with a switching frequency of 5 kHz.

The VSG-based frequency and voltage control is initiated during islanding operation, whereas during grid-connected operation VSC operates in grid-following mode, and active power flow is controlled to maintain the state-of-charge of BESS. The proposed VSG control for VSC is comparable to the characteristics of SG. This paper proposes swing-equation-based VSG control, the frequency of VSG is governed by Eqs. (5)–(7) [31]. Assuming that viscous damping (K_D) opposes the rotating shaft system of a synchronous machine and proportional-integral (PI) controller for regulating system frequency.

$$2H\frac{d\omega_{VSG}}{dt} = P_{mech.} - P_{VSG} \tag{5}$$

$$P_{mech.} - P_{ref.} = \frac{1}{D_p}(\omega_{ref.} - \omega_{pcc}) \tag{6}$$

$$\begin{aligned} 2H\frac{d\omega_{VSG}}{dt} &= P_{mech.} - P_{VSG} - K_D(\Delta\omega) \\ &\quad + K_{pf}(\Delta\omega) + (K_{if})\int(\Delta\omega.dt) \end{aligned} \tag{7}$$

where ω_{VSG}&P_{VSG} are the angular frequency and active power of VSG respectively. K_{pf}&K_{if} are the proportional and integral gain of frequency control of VSG respectively. ω_{pcc}&ω_{ref} are the angular frequency of PCC and reference respectively. D_p is the active power droop coefficient and $P_{mech.}$ is the mechanical power of VSG. H is the inertia constant of VSG in seconds. $\Delta\omega$ is the change in angular frequency of VSG.

The terminal voltage and reactive power control of VSG is generated based on the following equation.

$$E_{d-ref.} = V_{ref.} - D_q Q_{VSG} + K_{pv}(Q_{ref.} - Q_{VSG}) + K_{iv}\int (Q_{ref.} - Q_{VSG}).dt \tag{8}$$

where $K_{pv}\&K_{iv}$ are the proportional and integral gain of voltage control of VSG respectively.$Q_{ref.}$ and Q_{VSG} are the reactive power reference value and reactive power of VSG respectively. $E_{d-ref.}$ is the generated reference value of voltage in direct axis rotating frame. $V_{ref.}$ is the reference value of voltage required from VSC and D_q is the reactive power droop coefficient

The detailed explanation of voltage and current control strategy of VSC adopted for this work is provided in [32]. Also, it is assumed that inclusion of high value of line filters for large power electronics based VSC leads to high X/R ratio of microgrid. Such high values of X/R ratio results in inductive nature of microgrids and hence well known P/X and Q/V droop control strategy can be considered in proposed work so as to regulate the frequency and the voltage of the microgrid [32]. The active and reactive power droop coefficient can be calculated as;

$$D_p = \frac{2\pi(f_{max} - f_{min})}{P_{VSGmax}} \tag{9}$$

$$D_q = \frac{(V_{max} - V_{min})}{Q_{VSGmax}} \tag{10}$$

where $(f_{max} - f_{min})$ is the acceptable range of frequency variation for VSC. A frequency deviation of 5% from the nominal value of 50 Hz is considered in the proposed work. The acceptable limits for RoCoFmin and RoCoFmax are considered as 0 and 1 Hz/s respectively. P_{VSGmax} is the maximum requirement/available active power. Similarly, $(V_{max} - V_{min})$ is the acceptable range of voltage variation for VSC. For the present work 10% of voltage variation is considered.

The relation between value of instantaneous RoCoF just after any power disturbance (ΔP) occurred in system and inertia constant (H) can be stated as [33];

$$RoCoF = \frac{\Delta P}{P_{rated}} \frac{f_{ref}}{2H} \tag{11}$$

For a practical scenario, the inertia constant (H) is chosen wisely, such that RoCoF is maintained with the prescribed limits for any value of power disturbance in the system.

4.2. Adaptive parameters optimization framework

This paper proposes an adaptive parameters optimization framework for VSG through a coordinated two-level approach, wherein a day-ahead value of inertia is estimated at the first level using robust modelling, followed by adaptive intra-hour optimization of the VSG parameters at 5-minute intervals during islanding. The focus of the adaptive parameters optimization is to track uncertainties and provide fast frequency recovery under dynamic operating conditions by updating the parameters of VSG in a shorter time scale. The adaptive coordination framework is illustrated in Fig. 4. As can be observed from the figure, at the first level, MGCC receives day-ahead forecasts of hourly PV output and load. With the uncertainty input data, MGCC performs interval prediction to estimate the worst-case realization of uncertainty in 24 h of the following day. Accordingly, VSG parameters are computed for worst-case uncertainty occurrence, ensuring robust operation of VSG. During intra-day operation stage on the following day, as soon as islanding is detected, the VSG is initiated with robust values of the parameters computed day-ahead. Following this, the MGCC determines the expectation values of short-leading-time predictions of PV output and load, and performs an adaptive stochastic optimization of VSG parameters in intervals of 5-minutes.

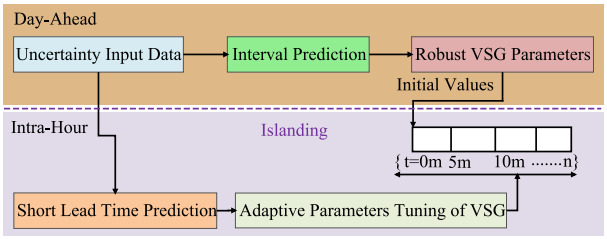

Fig. 4. Adaptive coordination framework.

4.3. Robust modelling of inertia

For day-ahead modelling of robust VSG parameters in the first level, worst-case uncertainties in solar PV output (P^{pv}) and load (P^{L}) are computed through mathematical representation using polyhedral uncertainty sets. The polyhedral uncertainty sets provide an appropriate trade-off between the accuracy and robustness of the solution, thereby ensuring computational efficiency. The general mathematical representation of the polyhedral uncertainty set U_a, is given as follows [34].

$$U_a = \left\{ \tilde{a}_{ij} = a_{ij} + \xi_{ij}\hat{a}_{ij} \middle| \sum_j \xi_{ij} \le \Gamma_i \right\} \tag{12}$$

where, $\tilde{a}_{ij}$ is the actual value of the uncertain variable; a_{ij} and $\hat{a}_{ij}$ are the nominal and maximum values of uncertainty occurrence; Γ is an adjustable parameter that signifies the level of robustness. The polyhedral uncertainty set for different values of Γ ($\Gamma_1 \le \Gamma_2$) is illustrated in Fig. 5. Thus, the polyhedral uncertainty set representation for worst-case uncertainty in PV output and load (φ^{pv} and φ^{l}) is obtained from (12) as follows.

$$U_{pv/l} = \left\{ \varphi^{pv/l} = P_f^{pv/l} + \xi^{pv/l} P_r^{pv/l} \middle| \sum_j \xi_j^{pv/l} \le \Gamma_{pv/l} \right\} \tag{13}$$

$$P_{min}^{pv/l} = P_f^{pv/l} - P_r^{pv/l}\Gamma_{pv/l} \tag{14}$$

$$P_{max}^{pv/l} = P_f^{pv/l} + P_r^{pv/l}\Gamma_{pv/l} \tag{15}$$

$$\mu_{pv/l}^{l} = 1 - \Gamma_{pv/l}\ ;\ \mu_{pv/l}^{l} = u + \Gamma_{pv/l} \tag{16}$$

where, $\varphi^{pv/l}$ are the worst-case uncertainty values of PV output and load, $P_{min/max}^{pv/l}$ are the minimum/maximum values of PV/load forecast, $P_f^{pv/l}$ are the forecast values of PV output/load, $P_r^{pv/l}$ is the nominal value of PV output/load, $\mu_{pv/l}^{l}$ and $\mu_{pv/l}^{u}$ are the lower and upper budgets of PV/load uncertainty sets respectively. $\Gamma_{pv/l}$ refers to the robustness adjustment parameter for PV output/load, which limits the per unit uncertainty occurrence. Thus, $\Gamma_{pv/l}$ corresponds to the values that $\xi^{pv/l}$ takes values from within the polyhedron shown in Fig. 5. Accordingly, the polyhedral uncertainty sets for φ^{pv} and φ^{l} are represented as follows.

$$U_{pv} = \{\varphi^{pv} \in \mathbb{R}^{n_{pv}} : P_{min}^{pv} \le P^{pv} \le P_{max}^{pv} \quad \mu_{pv}^{l} \le \frac{P^{pv}}{P_f^{pv}} \le \mu_{pv}^{u}\} \tag{17}$$

$$U_L = \{\varphi^{l} \in \mathbb{R}^{n_l} : P_{min}^{l} \le P^{l} \le P_{max}^{l} \quad \mu_{l}^{l} \le \frac{P^{l}}{P_f^{l}} \le \mu_{l}^{u}\} \tag{18}$$

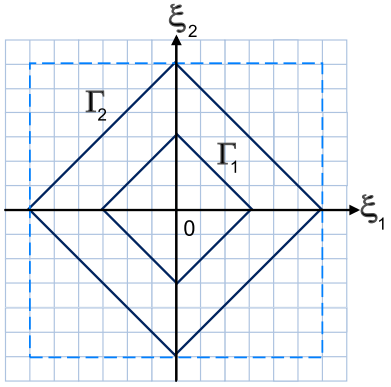

Fig. 5. Polyhedral uncertainty set.

4.4. Multi-objective optimization

The adaptive intra-hour optimization at the lower level is developed as a multi-objective optimization problem, wherein first objective ($g_1(x)$) refers to minimization of $RoCoF$, while the second objective ($g_2(x)$) refers to minimization of inertia constant. Since $RoCoF$ and H are inversely related as per (11), the overall optimization problem is composed of two contrasting objectives and solved using suitable solution algorithm. The two objectives are mathematically represented as follows.

$$\min g_1(x) = \min H \tag{19}$$

$$\min g_2(x) = \min RoCoF \tag{20}$$

subjected to the following constraints,

$$RoCoF^{min} \le RoCoF \le RoCoF^{max} \tag{21}$$

$$H^{min} \le H \le H^{max} \tag{22}$$

$$RoCoF = \frac{\Delta P}{P_r}\frac{f_o}{2H} \tag{23}$$

where, $(RoCoF/H)^{min}$ and $(RoCoF/H)^{max}$ refer to the minimum/maximum values of $RoCoF$ and H, P_r and f_o are the power and frequency ratings of the system, respectively. ΔP is dependent upon the real-time occurrence of P_{pv} and P_L which are inherently uncertain. The short-leading-time uncertainty in P_{pv} can be accurately represented by beta probability distribution function (PDF), given as follows [35].

$$f_{P_{pv}}(y) = y^{\alpha'-1}(1-y)^{\beta'-1}N_\beta \tag{24}$$

where, α' and β' refer to the shape parameters of beta PDF, N_β refers to a normalization factor, while y refers to the occurrence of uncertainty in P_{pv}. Similarly, stochastic uncertainty in load occurrence can be precisely represented by the normal PDF, given as follows.

$$f_{P_l}(y) = \frac{1}{\sqrt{2\pi(\sigma_l)^2}}exp(-\frac{(x-\mu_l)^2}{2\sigma_l^2}) \tag{25}$$

where, μ_l and σ_l refer to the mean value and standard deviation of load forecast, respectively.

The stochastic programming model has been developed to minimize the expectation values of the objective functions (19) and (20) in the presence of uncertainties. Let the objective functions be represented as $g_i(y_i) : y_i \in G_i(x,u), u \in U, x \in X$. Thus, the objective functions are mathematically reformulated as follows [35].

$$\min_{i=1,2} \mathbb{E}[H_i(x,u)] : x \in X, u \in U \tag{26}$$

where, u/U and x/X represent the uncertain decision and input variables/sets, respectively. $H_i(x,u)$ and $\mathbb{E}[H_i(x,u)]$ refer to the optimal value of the uncertain objective and its expected value, respectively.

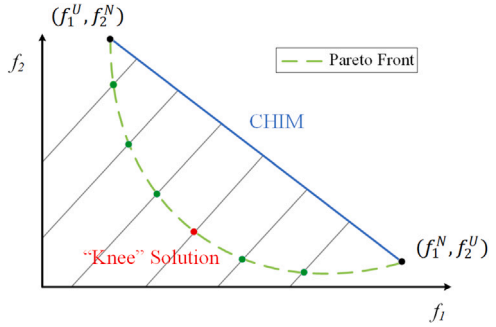

Fig. 6. Pareto front generation through normal boundary injection.

For solution of the stochastic programming model, it is formulated as a deterministic equivalent with the assumption that the uncertainty occurs in finite number of scenarios (N), each associated with an occurrence probability λ. Accordingly, the expectation function is expressed as follows.

$$\mathbb{E}[H_i(x,u)] = \sum_{n=1}^{N} \lambda_n H_i(x,u_n) \tag{27}$$

While the accuracy of the expectation function is increased with the number of uncertainty scenarios, the computational complexity also increases. Thus, a suitable trade-off is required in order to minimize the computational complexity while simultaneously ensuring solution accuracy. Accordingly, a finite number of uncertainty scenarios is generated using Monte Carlo simulation (MCS) and appropriately reduced to a smaller number (R) each associated with an occurrence probability λ_r, using the backward reduction technique to accurately represents the expected uncertainty. The expectation functions for the two objectives are thus obtained as follows.

$$\min_{y_1,\ldots,y_r} \sum_{r=1}^{R} \lambda_r' q_i(y_r);\ y_r \in G_i(u_r) \tag{28}$$

The proposed multi-objective optimization has been solved using the normal boundary intersection (NBI) solution algorithm. The NBI algorithm generates a shifted pay-off matrix M, whose nth column can be expressed as follows [36].

$$M = \begin{bmatrix} 0 & f_1^N - f_1^U \\ f_2^N - f_2^U & 0 \end{bmatrix} \tag{29}$$

Further, a convex hull of individual minima (CHIM) is generated $\{\phi\delta : \delta \in \Delta\}$, as shown in Fig. 6, where δ is a convex combination vector and Δ is a set of δ. Next, the NBI algorithm generates a normal to the CHIM as $\hat{n}$ and identifies points of intersection of the normal and the Pareto front. Finally, the algorithm searches for the intersection point closest to the origin, which is the "knee" solution as shown in Fig. 6. The knee solution is an optimal trade-off between the two contrasting objectives, and is considered as the best solution point from the Pareto.

Solution algorithm for the adaptive parameter tuning approach through multi-objective optimization is illustrated in Algorithm 1. During day-ahead operation, MGCC receives day-ahead forecast of PV output and load ($P_{t_u}^{pv}$ and $P_{t_u}^{l}$), where t_u refers to hourly timescale. Accordingly, robust VSG parameters H and $RoCoF$ are computed through worst-case uncertainty modelling using (17)–(18) for 24 h. As and when islanding occurs during real-time operation, the VSG is implemented with robust parameters for that particular hour which were computed one day-ahead. Simultaneously, the MGCC receives updated forecasts for short-leading-time uncertainties in PV output and load, $P_{t_l}^{pv}$ and $P_{t_l}^{l}$, where t_l refers to shorter time intervals of 5 min each. MGCC then performs stochastic modelling of uncertainties (ρ^{pv} and ρ^{l}) and implements multi-objective NBI-based optimization for R scenarios.

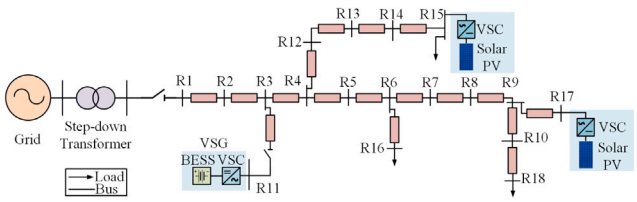

Fig. 7. Modified CIGRE network.

Finally, optimal stochastic output is obtained using (28) as adaptive values H' and $RoCoF'$, and VSG parameters are updated with the new values. The multi-objective stochastic optimization and adaptive VSG control is repeated every 5 min until grid-connection is restored.

Algorithm 1: Coordination framework for adaptive parameter optimization of VSG

1 ***Day-ahead operation***
2 Inputs: $P^{pv}_{t_u}$, $P^{l}_{t_u}$
3 **while** $t_u \in T$, *where* $T = [1, 24]$ **do**
4 Robust modelling of uncertainty using (17)-(18)
5 $\Delta P = |(P^{pv,f} - P^{l,f}) - (\varphi^{pv} - \varphi^{l})|$
6 Compute robust values H and $RoCoF$ (11)
7 **while** ***Islanded operation*** **do**
8 Inputs: $P^{pv}_{t_l}$, $P^{l}_{t_l}$, H, $RoCoF$
9 VSG control $\longrightarrow$ H and $RoCoF$
10 Stochastic modelling using (24)-(27)
11 Multi-objective NBI solution for (19)-(20)
12 Optimal stochastic output from (28) $\Longrightarrow$ Adaptive values H' and $RoCoF'$
13 Update VSG control $\longrightarrow$ H' and $RoCoF'$

5. Simulation results

The proposed adaptive parameters tuning strategy has been simulated on the modified CIGRE LV European test system as depicted in Fig. 7 [37]. A solar PV generation system of 4 kW each is connected at bus no. R15 and R17. BESS based VSC with VSG control is connected at bus no. R11 and loads are connected at bus no. R15, R16 and R18. The simulation is carried out on MATLAB/Simulink platform to evaluate the effectiveness of the proposed control strategy. The control regulates the system frequency through VSG-based VSC in islanding operation. The performance of proposed adaptive tuning control of VSG parameters considering forecasts for short-leading-time uncertainties in PV output and load is compared with VSG parameters evaluated through robust modelling. The robust modelling approach considers polyhedral uncertainty set for identification of worst operating conditions at any instant of time. The uncertainty budgets under different test conditions are shown in Table 1 considering a variation of 0%–15% of nominal value in solar PV power output and 0%–20% of nominal value in load power. Different test cases are considered and maximum deviation in active power is evaluated under different tests. It can be observed from the table that at any instant of time a maximum active deviation of 1.042 kW of active power is occurred for test no. 12. The value of H for worst case considering RoCoF value of 0.5 Hz/s is evaluated as 10.42 s. A 0.015 value of D_p is evaluated from (9) considering worst case condition of uncertainty.

Two different test cases are performed to evaluate the performance of layer 2 of coordinated control strategy. An islanding microgrid is considered and the VSG-based VSC connected at R11 regulates the voltage and frequency of the microgrid. The solar PV connected at R15 and R17 operates in grid following mode and follows the frequency of VSG-based VSC. In first case i.e. Case A, the active power of 2.78 kW is

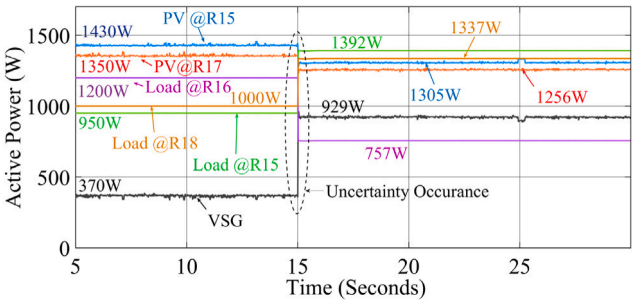

Fig. 8. Active power of loads and sources—Case A.

Table 1
Uncertainty budgets under different test conditions.

Test	γ^{l}_{PV}	γ^{u}_{PV}	ΔP_{PV}	γ^{l}_{L}	γ^{u}_{L}	ΔP_{L}	ΔP_{max}
1	0.95	1.05	137.5	0.95	1.05	157.5	295
2	0.90	1.10	275	0.90	1.10	315	590
3	0.85	1.15	412.5	0.85	1.15	472.5	885
4	0.95	1.05	137.5	0.80	1.20	630	767.5
5	0.90	1.10	275	0.95	1.05	157.5	432.5
6	0.85	1.15	412.5	0.90	1.10	315	727.5
7	0.95	1.05	137.5	0.85	1.15	472.5	610
8	0.90	1.10	275	0.80	1.20	630	905
9	0.85	1.15	412.5	0.95	1.05	157.5	570
10	0.95	1.05	137.5	0.90	1.10	315	452.5
11	0.90	1.10	275	0.85	1.15	472.5	747.5
12	0.85	1.15	412.5	0.80	1.20	630	1042.5

generated by from solar PV and 0.37 kW from VSG-based VSC to meet the load demand as shown in Fig. 8. During nominal conditions the system frequency is regulated at 50 Hz considering the initial values of VSG parameters from robust modelling as shown in Fig. 9. During nominal operation of islanding mode, the short lead time prediction of solar PV and load is done to evaluate VSG parameters and updated value of H = 4.97 s is given to VSG control. At time t = 15 s, an uncertainty of 0.559 kW in load and PV is occurred which causes a frequency deviation of 1.28 Hz and it restored in 1.79 s of time. However, 1.04 Hz of frequency deviation is observed for VSG parameters evaluated through robust control and frequency in restored in 3.27 s.

In another case i.e. Case B, the active power of 2.15 kW is generated by from solar PV and 2.05 kW from VSG-based VSC to meet the load demand as shown in Fig. 10. During nominal operation of islanding mode, the short lead time prediction of solar PV and load is done to evaluate VSG parameters and updated value of H = 6.99 s is given to VSG control. At time t = 15 s, an uncertainty of 0.904 kW in load and PV is occurred which causes a frequency deviation of 1.88 Hz and it restored in 3.39 s of time. However, 1.77 Hz of frequency deviation is observed for VSG parameters evaluated through robust control and frequency in restored in 3.75 s. The dynamic frequency response for case A and Case B is shown in Fig. 9 & 11 respectively. A comparison of performance indices for dynamic performance of VSG-based VSC under different simulation test conditions is shown in Table 1. It can thus, be concluded from the above simulation results that for operation under practical operating conditions, it is observed that maximum frequency deviation obtained with VSG operation through adaptive parameter tuning is slightly more as compared to that obtained with robust parameters. However, this is outweighed by significantly faster recovery time obtained with the adaptive stochastic optimization approach, as compared to the performance of parameters evaluated using day-ahead robust modelling (see Table 2).

6. Experimental results

In order to verify the effectiveness of the proposed control strategy, a laboratory-scale experiment setup has been developed as shown in

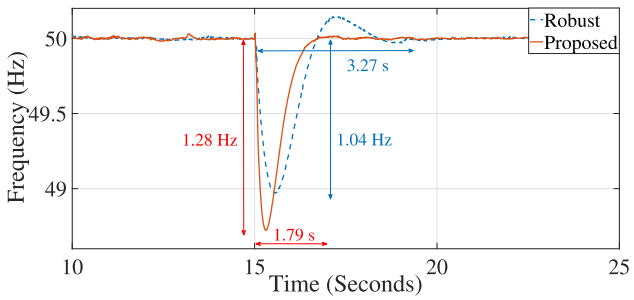

Fig. 9. Dynamic frequency response—Case A.

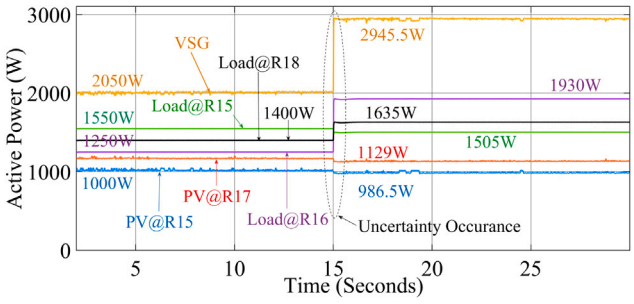

Fig. 10. Active power of loads and sources—Case B.

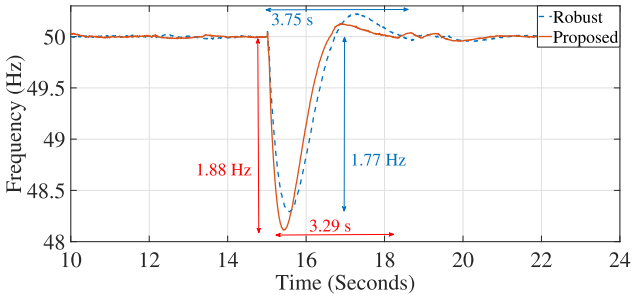

Fig. 11. Dynamic frequency response—Case B.

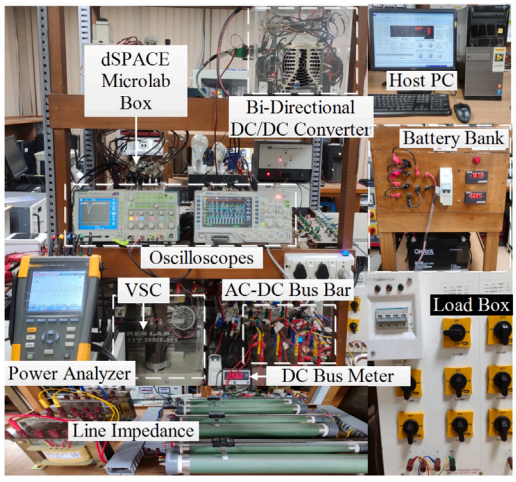

Fig. 12. Laboratory scale experimental setup.

Fig. 12. The BESS is connected to the DC bus of VSG control-based VSC using bi-directional DC–DC converter. The bi-directional DC–DC converter regulates the DC bus voltage of VSC and operates in grid forming mode using VSG control strategy. The dSPACE microlab box provides gate pulses to converters and sense the analog input from different voltage-current sensors at a sampling period of 50 μs. The system parameters considered in the experimental setup are depicted in Table 3.

Table 2
Dynamic performance of VSG-based VSC under different simulation test conditions.

Case A					
Control	ΔP (W)	$RoCoF$ (Hz/s)	H (s)	Δf_{max} (Hz)	Recovery time (s)
Robust	559	0.50	10.42	1.04	3.27
Proposed	559	0.55	4.97	1.28	1.79
Case B					
Robust	895.5	0.50	10.42	1.77	3.75
Proposed	895.5	0.66	6.99	1.88	3.29

Table 3
Experimental system parameters.

System parameters
BESS: No. of batteries = 14 No. s, Cap. of each batt. = 12 V, 65 AH **BDC:** C_{Bdc} = 1000 μF, L_{Bdc}= 1.66 mH, C_{DC} = 1200 μF
VSC: Capacity = 3 kVA, 415 V, L_f = 7.5 mH, C_f = 20 μF, R_f = 5 Ω $Step-upX'mer = 3-\phi$, 415 V, 25 A
Line Impedance: R = 0–3 Ω 20 A, L = 0–10 mH 15 A

6.1. Frequency control during islanded microgrid

This section handles the performance evaluation of the proposed adaptive parameters tuning strategy of VSG under different step changes in load. A BESS-based VSG control during islanding condition is considered in the experimental evaluation. The DC bus of VSC is regulated by BDC connected to BESS. VSG control is implemented to grid forming VSC which regulates the frequency and voltage of an islanded microgrid.

6.1.1. Dynamic response under variable inertia

In this case, the dynamic performance of system frequency is examined under variable inertia constant. The main objective of this case is to demonstrate the variation of f_{max} and recovery time of system frequency under different inertia constants. The VSC regulates system frequency at 50 Hz and balanced line voltages during normal operating condition as shown in Fig. 13. A resistive load of 0.5 kW is connected to VSC during nominal condition and VSC is operated at unity power factor (p.f.) as shown in Fig. 14.

A step change of 0.6 kW is made at time t = 2 s which causes variation of system frequency and is restored to its nominal value. The dynamic response of system frequency under different inertia constants is shown in Fig. 15. It can be observed from the dynamic response of frequency, that magnitude of frequency deviation reduces with an increase in system inertia constant, but an increase in inertia constant causes an increase in frequency recovery time. Therefore optimal values of VSG parameters are required for minimizing frequency deviation and faster restoration of system frequency. The comparison of performance indices for a fixed step change in load under different values of inertia constant is shown as Case A in Table 5.

6.1.2. Dynamic response under different loading conditions

The proposed adaptive parameter tuning approach evaluates the optimal values of VSG parameters under variable loading conditions. Initially, day-ahead optimization of VSG parameters is performed to evaluate robust values of VSG parameters considering worst-case uncertainty conditions. The day-ahead computed values of VSG parameters calculated from robust modelling of uncertainties is considered as initial values during islanding operation of microgrid. It can be observed

from Fig. 16, that for a step change of 0.87 kW in load (worst-case), 0.70 Hz/s value of $RoCoF$ and inertia constant of 10.27 s is calculated through robust modelling. At time t = 2 s, a step change of 0.87 kW is made and frequency deviation of 1.5 Hz is observed for robust VSG parameters. The frequency is restored to its nominal value in 3 s.

Similar worst-case loading condition is considered for evaluating the VSG parameters using the proposed adaptive stochastic optimization approach. $RoCoF$ value of 0.86 Hz/s and inertia constant of 7.99 s are obtained through the proposed intra-hour optimization approach. It is noted that a frequency deviation of 1.65 Hz and recovery time of 2.6 s is observed for VSG parameters obtained through adaptive stochastic optimization under the worst-case scenario. It can further be observed from Fig. 16 that the parameters obtained from the proposed adaptive optimization provide similar dynamic performance of frequency as compared to robust tuning, under worst-case scenario. The comparison of performance indices under worst-case scenario is shown as Case B in Table 5.

It must be noted that worst-case conditions are rarely observed in practice. As a result, robust values of VSG parameters are highly conservative for actual system operation. This necessitates adaptive tuning of VSG parameters considering real-time operating conditions, which has been performed in the proposed approach through intra-hour (5-minute) stochastic optimization. Accordingly, for a step load change of 0.6 kW, the VSG parameters are calculated as $RoCoF$ = 0.75 Hz/s and inertia constant = 6.99 s through the proposed adaptive tuning method. The step load change is made at time t = 2 s as shown in Fig. 17. A frequency deviation of 1 Hz with a recovery time of 3 s is observed for robust VSG parameters, with an inertia constant of 10.27 s as calculated through robust modelling. However, a frequency deviation of 1.1 Hz with a recovery time of 2.2 s is observed with adaptive optimization of inertia constant obtained as 6.99 s. Thus, it can be observed from the dynamic performance that the proposed adaptive tuning approach provides faster frequency restoration as compared to the VSG parameters obtained from day-ahead robust modelling. The comparison of performance indices under 0.6 kW step change in load is shown as Case C in Table 5.

In another case, the VSG parameters are evaluated for a step change of 0.292 kW using proposed adaptive parameter tuning approach. VSG parameters from the adaptive optimization approach are obtained as $RoCoF$ = 0.47 Hz/s and inertia constant = 4.97 s. These values are provided to VSG controller and frequency deviation of 0.6 Hz is observed with recovery time of 0.7 s. However, for VSG parameters calculated through day-ahead robust modelling, frequency deviation of 0.48 Hz and recovery time of 1.5 s are observed. The dynamic performance for both control strategies is shown in Fig. 18. The comparison of performance indices under 0.292 kW step change in load is shown as Case D in Table 5. It can thus, be concluded from the above experimental results that the performance of the parameters evaluated through proposed adaptive optimization are comparable to the performance observed with robust parameters for the worst-case scenarios. For operation under practical operating conditions other than the worst-case scenario, it is observed that maximum frequency deviation obtained with VSG operation through adaptive parameter tuning is slightly more as compared to that obtained with robust parameters. However, this is outweighed by significantly faster recovery time obtained with the adaptive stochastic optimization approach, as compared to the performance of parameters evaluated using day-ahead robust modelling.

6.1.3. Dynamic response under false data injection

In the past few years, events of cyber-attacks on power systems are increasing as smart grids and microgrids are prone to such events due to the presence of communication infrastructure. The operation of such electrical network is dependent upon data exchange through communication mediums such as Internet-of-Things, 5G communications etc. [38]. Unfortunately, because of the open wireless intrusion

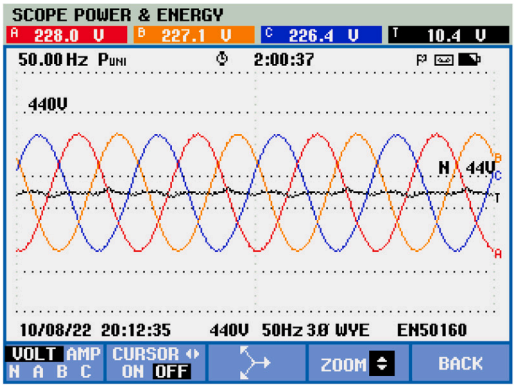

Fig. 13. Voltage waveform at PCC.

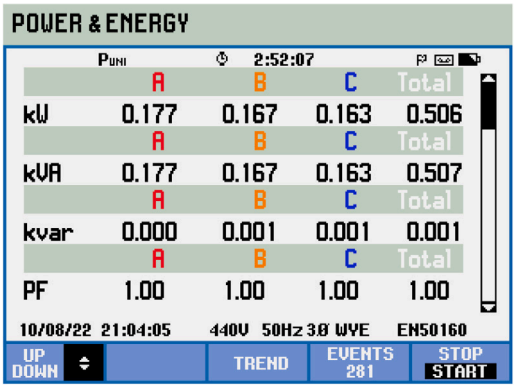

Fig. 14. VSC powers.

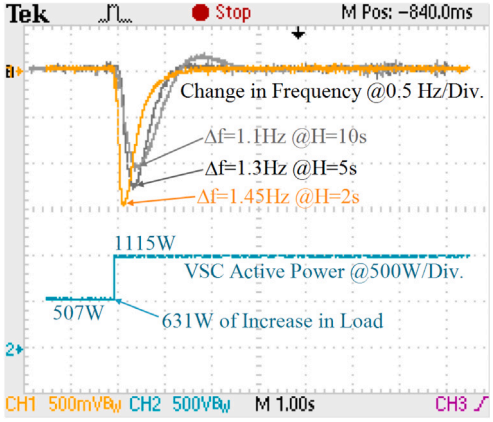

Fig. 15. Dynamic response-Case A.

interface, hackers are able to fudge the signals sent by weak devices (such remote terminal units), which leads to cyber threats and disrupts system stability [39]. In load frequency control system, the frequency signal is extremely important which can be targeted by hackers, falsifying such signals may affect the stability of the system. Cyber-attack can occur in multiple ways by replacing the measured value known as a replay attack, falsifying the measurement signal known as a false data injection attack etc. [38]. However, in this work, false data injection is considered to evaluate the performance of proposed strategy under cyber-attack. False data injection is classified into two types: extraneous attack and scaling attack. In this work, we have considered extraneous attack where hackers attempt to include disturbance in the measurement signals which can be a step, random, signum signal etc.

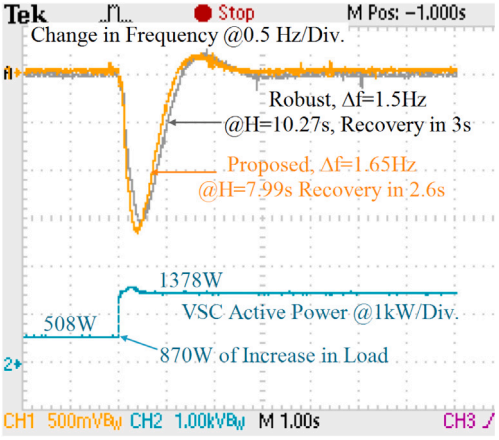

Fig. 16. Dynamic response-Case B.

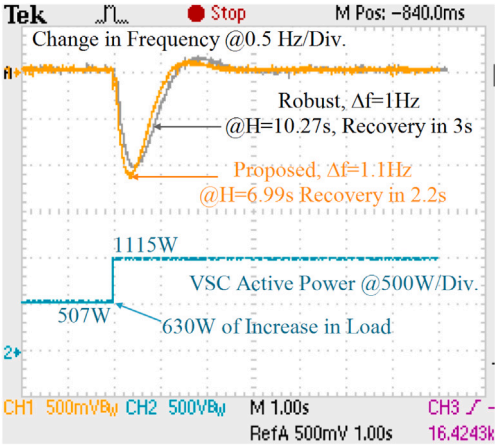

Fig. 17. Dynamic response-Case C.

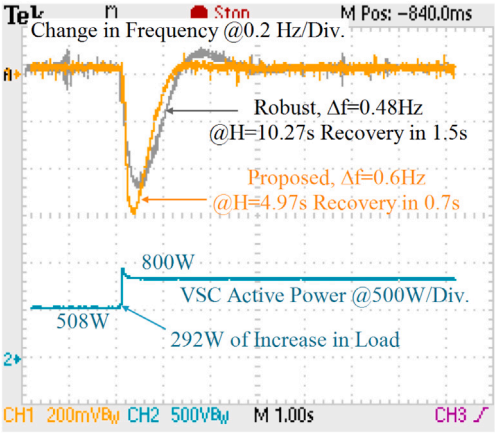

Fig. 18. Dynamic response-Case D.

A random signal (χ) generated through a random signal generator block in MATLAB/Simulink is added to the change in measured frequency signal ($\Delta f_{measured}$). The parameters of the random signal generator block are provided in Table 4. The net change in frequency (Δf_{net}) measurement observed by the load frequency controller is given as;

$$\Delta f_{net} = \Delta f_{measured} + \chi \tag{30}$$

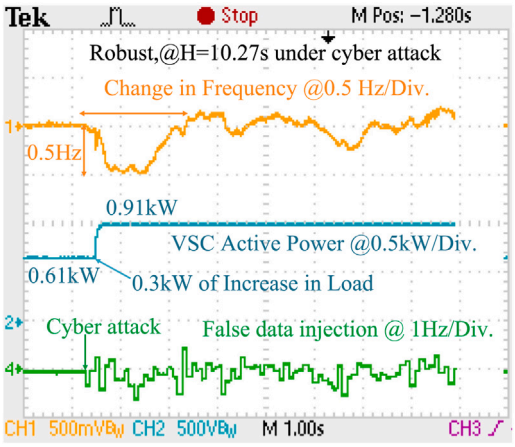

Fig. 19. Frequency response of robust control under false data injection.

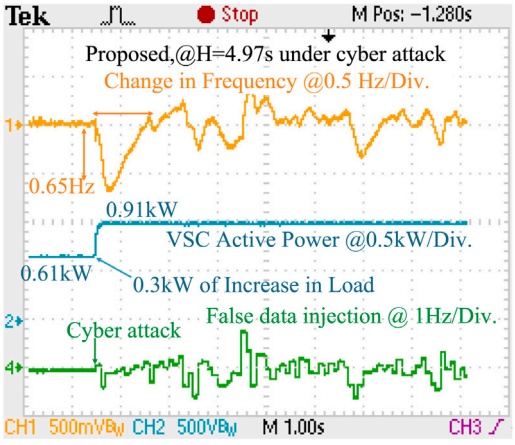

Fig. 20. Frequency response of proposed control under false data injection.

Table 4
Parameters of the random signal generator.

Variance	0.05
Mean	559
SampleTime	0.1 s

A resistive load of 0.61 kW is connected to VSG-based VSC and a step change of 0.3 kW along with false data injection-based cyber attack is observed as shown in Fig. 19. The step change in load power along with false data injection causes a frequency deviation of 0.5 Hz for robust control with an inertia constant of 10.27 s calculated through robust modelling and recovered in 1.1 s. The dynamic frequency response of robust control under false data injection is shown in Fig. 19. A similar test case is performed for the proposed control strategy and a frequency deviation of 0.65 Hz is observed for the proposed control with an inertia constant of 4.97 s calculated through adaptive parameters tuning. The frequency is restored in 0.5 s. The dynamic frequency response of the proposed control strategy under false data injection is shown in Fig. 20. It can be observed from the frequency responses that the proposed adaptive parameters tuning strategy provide fast frequency restoration under false data injection as compared to the robust control strategy which utilizes fixed parameters.

Table 5
Dynamic performance of VSG-based VSC under different experimental test conditions.

Case A					
Control	ΔP (W)	$RoCoF$ (Hz/s)	H (s)	Δf_{max} (Hz)	Recovery time (s)
H = 10 s	608	0.72	10	1.1	1.3
H = 5 s	608	0.72	5	1.3	0.8
H = 2 s	608	0.72	2	1.45	0.6
Case B					
Robust	870	0.70	10.27	1.50	3.0
Proposed	870	0.86	7.99	1.65	2.6
Case C					
Robust	608	0.70	10.27	1.00	3.0
Proposed	608	0.72	6.99	1.10	2.2
Case D					
Robust	292	0.70	10.27	0.48	1.5
Proposed	292	0.47	4.97	0.60	0.7
Case E					
Robust	292	0.70	10.27	0.5	1.1
Proposed	292	0.47	4.97	0.65	0.5

7. Conclusion

The paper proposes adaptive parameters tuning strategy for RES-integrated electrical microgrid systems. Accordingly, two-level optimization model has been developed to address the impacts of real-time uncertainties arising due to RES integration, as well as to maintain network voltage and frequency stability under different modes of microgrid operation. A virtual inertia support through VSG-based control of VSC during islanded mode of operation. It develops a two-level adaptive optimization framework for determining robust VSG parameters as initialization values during islanding conditions. This is followed by a novel adaptive parameter optimization approach performed during islanding in 5-minute intervals. The adaptive optimization is formulated as a stochastic programming approach, based on the expectation of short-leading-time uncertainties in PV output and load, and solved through NBI-based multi-objective solution algorithm. The effectiveness of the proposed adaptive tuning strategy is verified through extensive simulations and laboratory-scale experiments. The results validate the superior performance of the proposed strategy for fast frequency regulation under system uncertainties as compared to the parameters calculated through robust modelling. The performance of the proposed strategy is also evaluated under cyber-attack considering false data injection. The proposed adaptive parameters tuning strategy provides adaptive parameters of VSG in real-time operation with faster frequency restoration.

CRediT authorship contribution statement

Himanshu Grover: Writing – review & editing, Writing – original draft, Validation, Methodology, Conceptualization. **Sumedha Sharma:** Writing – review & editing, Writing – original draft, Visualization, Methodology, Formal analysis, Conceptualization. **Ashu Verma:** Writing – review & editing, Validation, Supervision, Resources, Investigation. **M.J. Hossain:** Writing – review & editing, Visualization, Validation, Supervision, Investigation, Conceptualization. **Innocent Kamwa:** Writing – review & editing, Visualization, Validation, Supervision.

Declaration of competing interest

The authors declare that they have no known competing financial interests or personal relationships that could have appeared to influence the work reported in this paper.

Data availability

No data was used for the research described in the article.

References

[1] B. Pournazarian, R. Sangrody, M. Lehtonen, G.B. Gharehpetian, E. Pouresmaeil, Simultaneous optimization of virtual synchronous generators parameters and virtual impedances in islanded microgrids, IEEE Trans. Smart Grid (2022) 1.

[2] C. O'Malley, L. Badesa, F. Teng, G. Strbac, Probabilistic scheduling of UFLS to secure credible contingencies in low inertia systems, IEEE Trans. Power Syst. 37 (4) (2021) 2693–2703.

[3] S. Gordon, C. Mcgarry, K. Bell, J. Tait, Impact of low inertia and high distributed generation on the effectiveness of under frequency load shedding schemes, IEEE Trans. Power Deliv. (2021) 1.

[4] H. Grover, A. Verma, T. Bhatti, DOBC-based frequency & voltage regulation strategy for PV-diesel hybrid microgrid during islanding conditions, Renew. Energy 196 (2022) 883–900.

[5] A. Fathi, Q. Shafiee, H. Bevrani, Robust frequency control of microgrids using an extended virtual synchronous generator, IEEE Trans. Power Syst. 33 (6) (2018) 6289–6297.

[6] B. Long, Y. Liao, K.T. Chong, J. Rodríguez, J.M. Guerrero, MPC-controlled virtual synchronous generator to enhance frequency and voltage dynamic performance in islanded microgrids, IEEE Trans. Smart Grid 12 (2) (2021) 953–964.

[7] C. Liu, X. Wang, Y. Ren, X. Wang, J. Zhang, A novel distributed secondary control of heterogeneous virtual synchronous generators via event-triggered communication, IEEE Trans. Smart Grid 13 (6) (2022) 4174–4189.

[8] Y. Qi, T. Yang, J. Fang, Y. Tang, K.R.R. Potti, K. Rajashekara, Grid inertia support enabled by smart loads, IEEE Trans. Power Electron. 36 (1) (2021) 947–957.

[9] U. Tamrakar, D. Shrestha, M. Maharjan, B.P. Bhattarai, T.M. Hansen, R. Tonkoski, Virtual inertia: Current trends and future directions, Appl. Sci. 7 (7) (2017).

[10] H. Han, X. Hou, J. Yang, W. Jifa, M. Su, J. Guerrero, Review of power sharing control strategies for islanding operation of AC microgrids, IEEE Trans. Smart Grid 7 (2015) 1.

[11] J. Li, B. Wen, H. Wang, Adaptive virtual inertia control strategy of VSG for micro-grid based on improved bang-bang control strategy, IEEE Access 7 (2019) 39509–39514.

[12] J. Chen, M. Liu, T. O'Donnell, Replacement of synchronous generator by virtual synchronous generator in the conventional power system, in: 2019 IEEE Power & Energy Society General Meeting, PESGM, 2019, pp. 1–5.

[13] M.A. Torres L., L.A.C. Lopes, L.A. Morán T., J.R. Espinoza C., Self-tuning virtual synchronous machine: A control strategy for energy storage systems to support dynamic frequency control, IEEE Trans. Energy Convers. 29 (4) (2014) 833–840.

[14] M. Torres, L.A.C. Lopes, Virtual synchronous generator control in autonomous wind-diesel power systems, in: 2009 IEEE Electrical Power & Energy Conference, EPEC, 2009, pp. 1–6.

[15] K.R. Vasudevan, V.K. Ramachandaramurthy, T.S. Babu, A. Pouryekta, Synchronverter: A comprehensive review of modifications, stability assessment, applications and future perspectives, IEEE Access 8 (2020) 131565–131589.

[16] A. Suvorov, A. Askarov, A. Kievets, V. Rudnik, A comprehensive assessment of the state-of-the-art virtual synchronous generator models, Electr. Power Syst. Res. 209 (2022) 108054.

[17] A. Suvorov, A. Askarov, Y. Bay, B. Maliuta, A. Achitaev, K. Suslov, Comparative small-signal stability analysis of voltage-controlled and enhanced current-controlled virtual synchronous generators under weak and stiff grid conditions, Int. J. Electr. Power Energy Syst. 147 (2023) 108891.

[18] S. D'Arco, J.A. Suul, O.B. Fosso, A virtual synchronous machine implementation for distributed control of power converters in SmartGrids, Electr. Power Syst. Res. 122 (2015) 180–197.

[19] V. Mallemaci, F. Mandrile, S. Rubino, A. Mazza, E. Carpaneto, R. Bojoi, A comprehensive comparison of virtual synchronous generators with focus on virtual inertia and frequency regulation, Electr. Power Syst. Res. 201 (2021) 107516.

[20] A. Suvorov, A. Askarov, N. Ruban, V. Rudnik, P. Radko, A. Achitaev, K. Suslov, An adaptive inertia and damping control strategy based on enhanced virtual synchronous generator model, Mathematics 11 (18) (2023).

[21] H. Grover, A. Verma, T. Bhatti, M.J. Hossain, Frequency regulation scheme based on virtual synchronous generator for an isolated microgrid, in: 2020 International Conference on Power, Instrumentation, Control and Computing, PICC, 2020, pp. 1–6.

[22] J. Chen, M. Liu, F. Milano, T. O'Donnell, Adaptive virtual synchronous generator considering converter and storage capacity limits, CSEE J. Power Energy Syst. 8 (2) (2022) 580–590.

[23] H. Wu, X. Ruan, D. Yang, X. Chen, W. Zhao, Z. Lv, Q.-C. Zhong, Small-signal modeling and parameters design for virtual synchronous generators, IEEE Trans. Ind. Electron. 63 (7) (2016) 4292–4303.

[24] H. Xu, C. Yu, C. Liu, Q. Wang, X. Zhang, An improved virtual inertia algorithm of virtual synchronous generator, J. Mod. Power Syst. Clean Energy 8 (2) (2020) 377–386.

[25] M. Li, W. Huang, N. Tai, L. Yang, D. Duan, Z. Ma, A dual-adaptivity inertia control strategy for virtual synchronous generator, IEEE Trans. Power Syst. 35 (1) (2020) 594–604.
[26] D. Li, Q. Zhu, S. Lin, X.Y. Bian, A self-adaptive inertia and damping combination control of VSG to support frequency stability, IEEE Trans. Energy Convers. 32 (1) (2017) 397–398.
[27] X. Hou, Y. Sun, X. Zhang, J. Lu, P. Wang, J.M. Guerrero, Improvement of frequency regulation in VSG-based AC microgrid via adaptive virtual inertia, IEEE Trans. Power Electron. 35 (2) (2020) 1589–1602.
[28] F.S. Rahman, T. Kerdphol, M. Watanabe, Y. Mitani, Optimization of virtual inertia considering system frequency protection scheme, Electr. Power Syst. Res. 170 (2019) 294–302.
[29] M. Hajiakbari Fini, M.E. Hamedani Golshan, Determining optimal virtual inertia and frequency control parameters to preserve the frequency stability in islanded microgrids with high penetration of renewables, Electr. Power Syst. Res. 154 (2018) 13–22.
[30] J. Liu, M. Hossain, J. Lu, F. Rafi, H. Li, A hybrid AC/DC microgrid control system based on a virtual synchronous generator for smooth transient performances, Electr. Power Syst. Res. 162 (2018) 169–182.
[31] F. Gao, M.R. Iravani, A control strategy for a distributed generation unit in grid-connected and autonomous modes of operation, IEEE Trans. Power Deliv. 23 (2) (2008) 850–859.
[32] M.S. Rahman, M. Hossain, J. Lu, Coordinated control of three-phase AC and DC type EV–ESSs for efficient hybrid microgrid operations, Energy Convers. Manage. 122 (2016) 488–503.
[33] Inertia and rate of change of frequency (RoCoF), version 17, in: International Series of Monographs on Physics, European Network of Transmission System Operators for Electricity, 2020.
[34] S. Sharma, A. Verma, Y. Xu, B.K. Panigrahi, Robustly coordinated bi-level energy management of a multi-energy building under multiple uncertainties, IEEE Trans. Sustain. Energy 12 (1) (2021) 3–13.
[35] S. Sharma, Y. Xu, A. Verma, B.K. Panigrahi, Time-coordinated multienergy management of smart buildings under uncertainties, IEEE Trans. Ind. Inform. 15 (8) (2019) 4788–4798.
[36] C. Zhang, Y. Xu, Z.Y. Dong, R. Zhang, Multi-objective adaptive robust voltage/VAR control for high-PV penetrated distribution networks, IEEE Trans. Smart Grid 11 (6) (2020) 5288–5300.
[37] CIGRE Task Force C6. 04.02, Benchmark Systems for Network Integration of Renewable and Distributed Energy Resources, International Council on Large Electric Systems Paris, France, 2014.
[38] D.K. Mishra, P.K. Ray, L. Li, J. Zhang, M. Hossain, A. Mohanty, Resilient control based frequency regulation scheme of isolated microgrids considering cyber attack and parameter uncertainties, Appl. Energy 306 (2022) 118054.
[39] C. Chen, K. Zhang, K. Yuan, L. Zhu, M. Qian, Novel detection scheme design considering cyber attacks on load frequency control, IEEE Trans. Ind. Inform. 14 (5) (2018) 1932–1941.